Electronic Supplementary Material

Highly stable and efficient non-precious metal electrocatalysts of tantalum dioxyfluoride for oxygen evolution reaction

Xin Yue [a, b] , Yanshuo Jin [a], and Pei Kang Shen [a, b] *

[q] School of Materials Science and Engineering, Sun Yat-sen University, Guangzhou, 510275, P. R. China.

[b] Collaborative Innovation Center of Sustainable Energy Materials, Guangxi University, Nanning 530004, P. R. China.

Experimental

Materials synthesis

TaO_2F/[g]C was synthesized by a ion adsorbed method: macroreticular weak basic styrene type anion exchange resin (10 g, D301, AR, > 99%, Shanghai Hualing Co. Ltd., China) was firstly adsorbed with sodium hexanitrocobaltate (1000 mL, 0.1 M $Na_3Co(NO_2)_6$, Aladding Chemistry Co. Ltd., China) solution. Then, the resin complex was stirred with potassium heptafluorotantalate (1.39 mM K_2TaF_7, Aladding Chemistry Co. Ltd., China) in 500 mL hot water for 5 hours. The resulting resin complex was then sintered at 1000 °C for 2 h under a pure N_2 flow. After slowly cooling down to room temperature, the product was ground and treated with 1 mol L^{-1}

HCl solution to remove cobalt and other impurities. After washing in deionized water and drying, TaO_2F/gC catalysts were stored for further characterizations.

As known, various tantalum compounds are insoluble and tantalum based chlorides and fluorides are best candidates as tantalum precursor for the same synthesizing process in this work [S1]. This is the reason why various Ta_2O_5 supported on carbon materials were synthesized through physical mixing methods [S2-S4]. Therefore, Ta_2O_5/CC (Ta_2O_5 supported on CC) was synthesized through a direct ball milling method: 317 mg Ta_2O_5 powder and 683 mg CC were treated by ball-milling for 6 h. Then, the product was treated with 1 mol L^{-1} HCl solution to remove impurities and washed in deionized water and drying,

Characterizations

X-ray diffraction (XRD) measurements were carried out on a D/Max-IIIA (Rigaku Co., Japan) employing Cu Kα (λ= 0.15406 nm) as the radiation source at 40 kV and 40 mA with a scanning rate of 8° min^{-1}. Morphologies of TaO_2F/gC were observed by Transmission Electron Microscopy (TEM) investigations on a FEI Tecnai G2 F30 operating at 300 kV. Raman analysis was performed on a micro-Raman spectrometer (Renishaw inVia, U.K.). X-ray photoelectron spectroscopy (XPS) measurements were carried out on a XPS apparatus (ESCALAB 250, Thermo-VG Scientific Ltd.). The thermal gravimetric (TG) analysis was carried out on Thermogravimetry coupled with Fourier transform infrared spectrometry (NETZSCH-Feinmahltechnik GmbH, Selb).

Electrochemical measurements

Electrochemical measurements were conducted on a Bio-Logic VMP3 potentiostat in a three-electrode cell by using a reversible hydrogen electrode (RHE) as the reference electrode and a graphite rod as the counter electrode. The working electrode was a glassy carbon electrode with diameter of 5 mm (ϕ = 5 mm). TaO_2F/gC, $KTaO_3$ (CAS: 12030-91-0), Ta_2O_5 (CAS: 1314-61-0) and CC electrocatalysts (10.0 mg) were dispersed in 1.5 mL ethanol and 0.5 mL Nafion (0.5 wt%, DuPont, USA) solution, respectively. The resulting mixture was then ultrasonicated for 45 min until obtain a well dispersed ink. Electrocatalysts ink was transferred to the surface of the work electrode. Then, to obtain an electrocatalysts thin film on electrode, the work electrode was dried under infrared lamp. Loadings of electrocatalysts on work electrode were 2.55 mg cm^{-2}. The electrochemical tests were performed in 1 M $HClO_4$ solution at 25 ^oC.

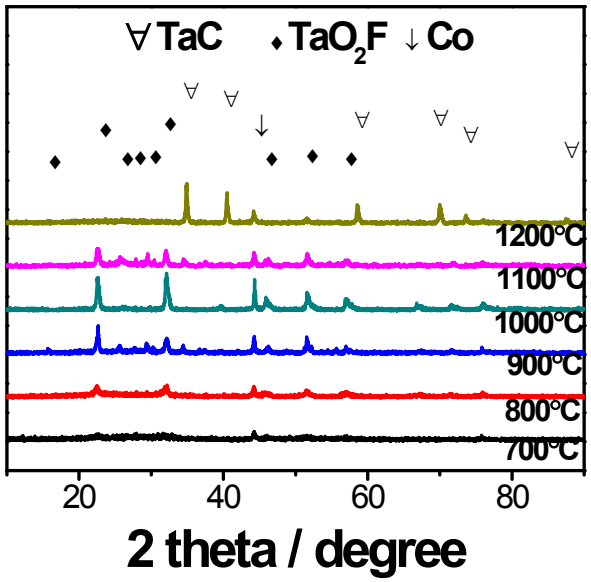

Fig. S1 XRD patterns of resin complexes sintered at different temperature under N_2 atmosphere.

XRD patterns of Ta_2O_5 and Ta_2O_5/CC were shown in Fig. S2a, indicating that the Ta_2O_5 phase is not changed after ball-milling process and impurities, such as iron, has been removed. Graphite (002) peak is too weak to be observed from XRD pattern.

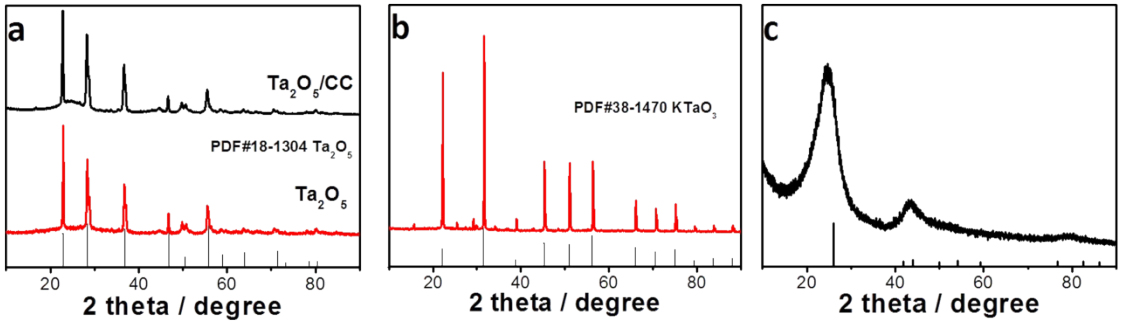

Fig. S2 XRD patterns of (a) Ta_2O_5/CC and Ta_2O_5, (b) $KTaO_3$and (c) CC.

XPS spectra of $KTaO_3$ were shown in Fig. S3. Doublet binding energy (BE) peaks position at 26.3 and 28.3 eV are assigned to $Ta_{7/2}$ and $Ta_{5/2}$ orbitals, indicating the existence of Ta-O bond identical to that of tantalum oxides [S5]. The peak position at ~ 501 eV in O 1s spectrum corresponds to Ta-O bond [S6, S7] (Fig. S3b). The peak position at 293.3 eV and 295.5 eV are attributed to the K-O bond in K 2p spectrum [S8] (Fig. S3c). F element has been not found in F 1s spectrum (Fig. S3d).

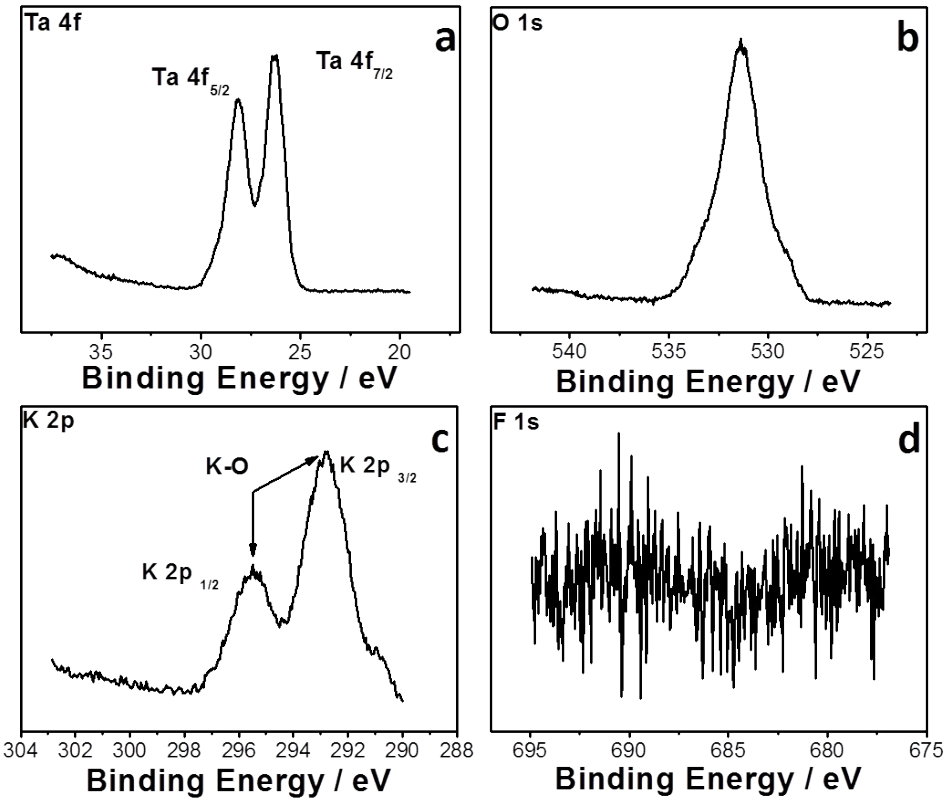

Fig. S3 XPS Spectra of $KTaO_3$.

XPS spectra of Ta_2O_5 were shown in Fig. S4. Doublet binding energy (BE) peaks position at 26.3 and 28.3 eV are assigned to $Ta_{7/2}$ and $Ta_{5/2}$ orbitals, indicating the existence of Ta-O bond identical to that of tantalum oxides [S5]. The peak position at ~ 501 eV in O 1s spectrum corresponds to Ta-O bond [S6, S7] (Fig. S4b).

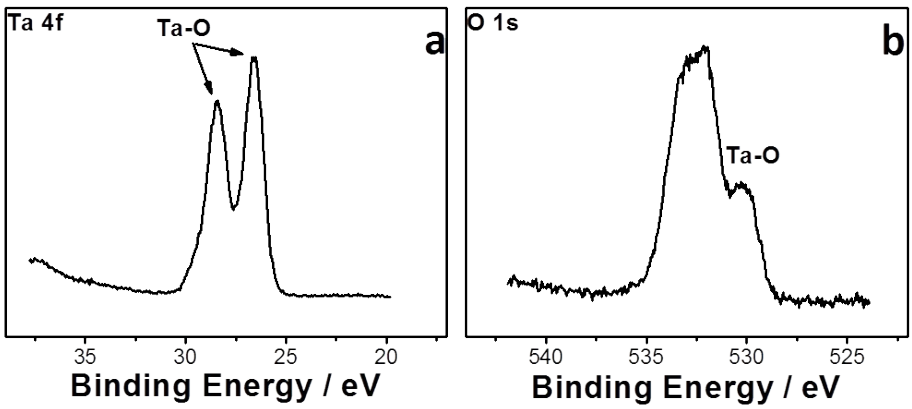

Fig. S4 XPS spectra of Ta_2O_5.

Loadings of electrocatalysts on electrode were 2.55 mg cm^{-2} in this work. However, as active composition, the loading of TaO_2F on gC was 31.7%, proved by TG analysis, indicating that loadings of TaO_2F on electrode was ~ 0.81 mg cm^{-2}. For comparison, Ta_2O_5 (with loadings on electrode of 0.81 and 2.55 mg cm^{-2}) and Ta_2O_5/CC (with loadings of Ta_2O_5 on electrode of 0.81 mg cm^{-2}) as electrocatalysts for OER was measured in 1 M KOH with scan rate of 1 mV s^{-1} at 25 °C (Fig. S5a). All polarization curves have been *iR*-corrected. Onset potentials of Ta_2O_5 with different loadings were as same as Ta_2O_5/CC (1.58 V *vs*. RHE). However, the current density of Ta_2O_5/CC at 1.80 V *vs*. RHE is 14.7 mA cm^{-2}, larger than that of Ta_2O_5 (9.0 mA cm^{-2}, with loadings on electrode of 0.81 mg cm^{-2}). It means that CC with better conductivity improves charge transfer properties of electrocatalysts and promotes the catalytic activity for OER on Ta_2O_5. Furthermore, Tafel slope of Ta_2O_5/CC is 112 mV/dec, as same as Ta_2O_5 (0.81 mg cm^{-2}) (116 mV/dec). However, the exchange current density (j_0) of Ta_2O_5/CC is 2.097×10^{-4} mA cm^{-2}, significantly larger than that of Ta_2O_5 (0.81 mg cm^{-2}) (1.346×10^{-4} mA cm^{-2}) indicating improvement of catalytic activity by supporting on conductive carbon materials (Fig.S5b).

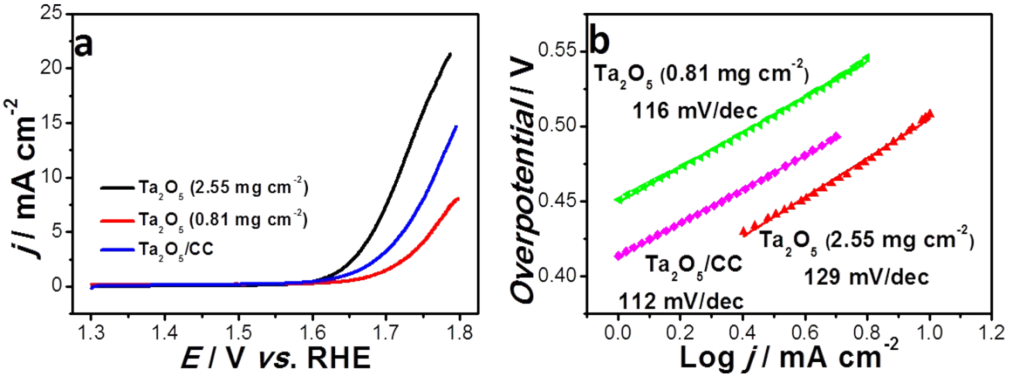

Fig. S5 (a) Polarization curves of Ta_2O_5 (with loadings on electrode of 0.81 and 2.55

mg cm^{-2}) and Ta_2O_5/CC electrocatalysts for OER in 1 M KOH with scan rate of 1 mV s^{-1} at 25 ^oC, (b) Tafel plots of Ta_2O_5 (with loadings on electrode of 0.81 and 2.55 mg cm^{-2}) and Ta_2O_5/CC electrocatalysts for OER.

Ta_2O_5/CC electrocatalysts exhibited lowest R_{ct} value (726 Ω at 1.60 V *vs.* RHE and only 13 Ω at 1.80 V *vs.* RHE) than Ta_2O_5, indicating much faster electron transportation on Ta_2O_5/CC electrocatalysts, attributing to high conductivity of CC (Fig. S6e). Conductive CC has been found to promote catalytic activity of Ta_2O_5 by improvement of charge transfer property. However, the onset potential and Tafel slope of Ta_2O_5/CC were not improved. It means that the intrinsic catalytic activity of Ta_2O_5 play a more important role in catalytic reaction.

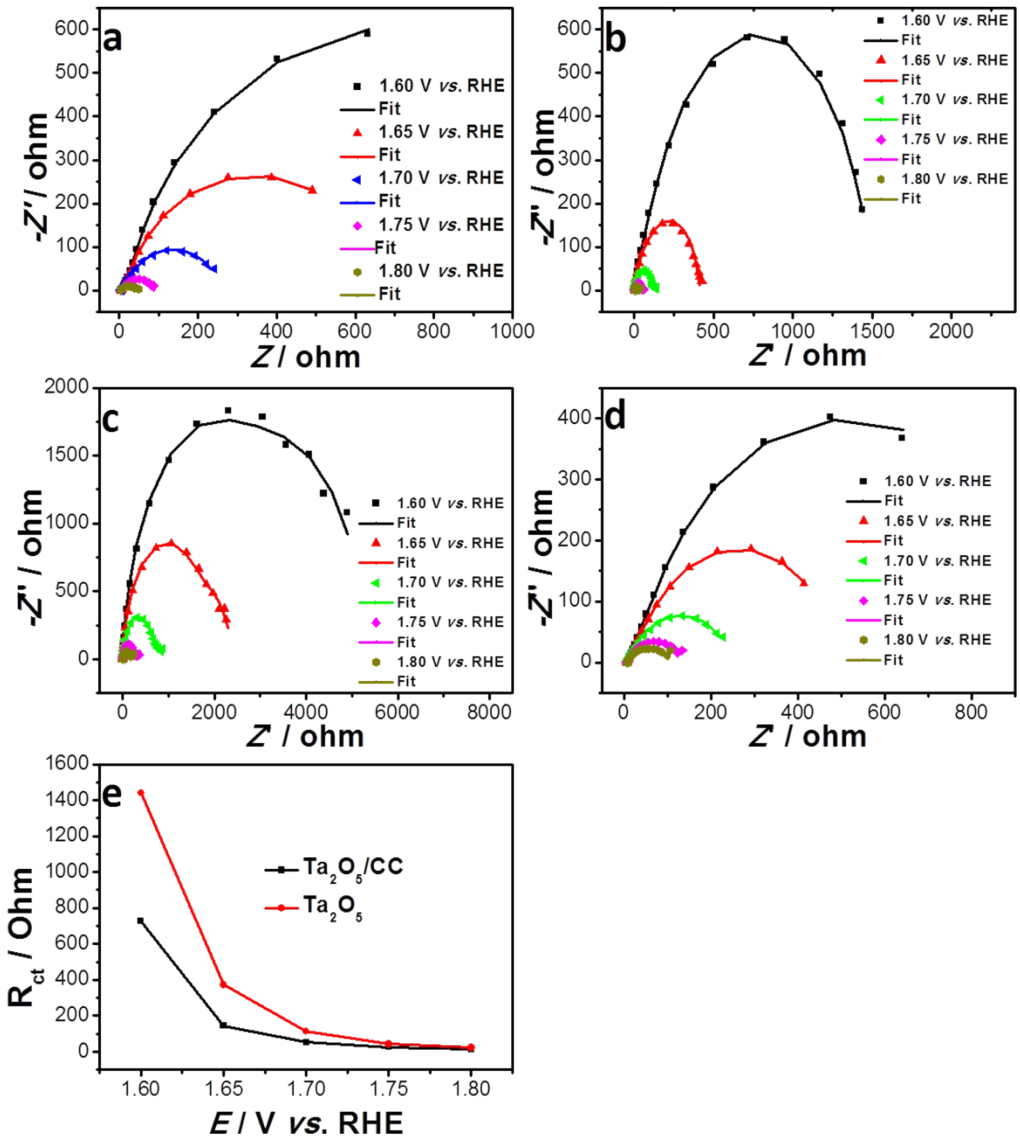

Fig. S6 Nyquist plots and fittings for impedance response of Ta_2O_5/CC, Ta_2O_5, $KTaO_3$ and CC electrocatalysts for OER. (e) relationship between charge-transfer resistance (R_{ct}) and overpotential of Ta_2O_5/CC and Ta_2O_5 electrocatalysts for OER,.

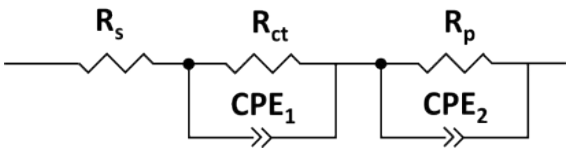

Fig. S7 A two-time constant model for fitting the EIS response of OER.

Table S1 OER performances of various transition metal oxides.

Electrocatalysts	Electrolyte	Onset potential / V *vs.* RHE	Overpotential @ specific current density	Tafel slop / mV dec^{-1}	J_0 / mA cm^{-2}	Ref.
Fe_3O_4	1 M KOH	N/A	650 mV @ 0.2 mA cm^{-2}	43	N/A	Int. J. Electrochem. Sci., 2012, 7, 15
Mn_3O_4	1 M KOH	N/A	>600 mV @ 3 mA cm^{-2}	60	N/A	RSC Adv., 2016, 6, 2019 – 2023
Co_3O_4	1 M KOH	N/A	400 mV @ 10 mA cm^{-2}	49	N/A	Chem. Mater., 2012, 24, 3567 –

						3573
MnOOH	0.M KOH/LiOH	N/A	550 mV @ 5 mA cm^{-2}	N/A	N/A	Nat. Mater., 2012, 11, 550 – 557
FeOOH	0.M KOH/LiOH	N/A	525 mV @ 5 mA cm^{-2}	N/A	N/A	Nat. Mater., 2012, 11, 550 – 557
CoOOH	0.M KOH/LiOH	N/A	450 mV @ 5 mA cm^{-2}	N/A	N/A	Nat. Mater., 2012, 11, 550 – 557
NiOOH	0.M KOH/LiOH	N/A	375 mV @ 5 mA cm^{-2}	N/A	N/A	Nat. Mater., 2012, 11, 550 – 557
TaO_2F/gC	1 M KOH	1.48	360 mV @ 10 mA cm^{-2}	78	1.402×10^{-3}	This work
Ta_2O_5	1 M KOH	1.58	480 mV @ 10 mA cm^{-2}	129	1.328×10^{-3}	This work
Ta_2O_5/CC	1 M KOH	1.58	530 mV @ 10 mA cm^{-2}	112	2.097×10^{-4}	This work
$KTaO_3$	1 M KOH	1.58	N/A	276	4.799×10^{-4}	This work
CC	1 M KOH	>1.	N/A	171	2.709×10^{-4}	This work

		60				

S1. A. Agulyansky, The chemistry of tantalum and niobium fluoride compounds, Elsevier, 2004, 8-10.

S2. X. Lv, W. Fu, C. Hu, Y. Chen and W. Zhou, *RSC Adv.*, 2012, **3**, 1753-1757.

S3. L. Mao, S. Zhu, J. Ma, D. Shi, Y. Chen, Z. Chen, C. Yin, Y. Li and D. Zhang, *Nanotechnology*, 2014, **25**, 215401.

S4. H. Sun, S. Liu, S. Liu and S. Wang, *Appl. Catal. B Environ.*, 2014, **146**, 162-168.

S5. L. Xu, H. Gong, L. Deng, F. Long, Y. Gu and J. Guan, *ACS Appl. Mater. Inter.*, 2016, **8**, 9395-9404.

S6. X Yue, C. He, C. Zhong, Y. Chen, S. P. Jiang and P. K. Shen, *Adv. Mater.*, 2016, **28**, 2163-2169.

S7. X. Yue and P. K. Shen, *Electrochim. Acta*, 2017, **227**, 267–274.

S8. N. Feng, *Sci. Rep.*, 2014, **4**, 3987.